



HAL
open science

Pattern formation in the nonlinear Schrödinger equation with competing nonlocal nonlinearities

F Maucher, T Pohl, W Krolikowski, Stefan Skupin

► To cite this version:

F Maucher, T Pohl, W Krolikowski, Stefan Skupin. Pattern formation in the nonlinear Schrödinger equation with competing nonlocal nonlinearities. *Optical Data Processing and Storage*, 2017, 3, pp.13 - 19. 10.1515/odps-2017-0003 . hal-01560999

HAL Id: hal-01560999

<https://hal.science/hal-01560999>

Submitted on 12 Jul 2017

HAL is a multi-disciplinary open access archive for the deposit and dissemination of scientific research documents, whether they are published or not. The documents may come from teaching and research institutions in France or abroad, or from public or private research centers.

L'archive ouverte pluridisciplinaire **HAL**, est destinée au dépôt et à la diffusion de documents scientifiques de niveau recherche, publiés ou non, émanant des établissements d'enseignement et de recherche français ou étrangers, des laboratoires publics ou privés.

F. Maucher*, T. Pohl, W. Krolikowski, and S. Skupin

Pattern formation in the nonlinear Schrödinger equation with competing nonlocal nonlinearities

DOI 10.1515/odps-2017-0003

Received February 13, 2017; revised April 9, 2017; accepted May 1, 2017

Abstract: We study beam propagation in the framework of the nonlinear Schrödinger equation with competing Gaussian nonlocal nonlinearities. We demonstrate that such system can give rise to self-organization of light into stable states of trains or hexagonal arrays of filaments, depending on the transverse dimensionality. This long-range ordering can be achieved by mere unidirectional beam propagation. We discuss the dynamics of long-range ordering and the crucial role which the phase of the wavefunction plays for this phenomenon. Furthermore we discuss how transverse dimensionality affects the order of the phase-transition.

Keywords: nonlinear Schrödinger equation, self-organization, competing nonlocal nonlinearities

1 Introduction

Pattern formation constitutes one of the most fascinating phenomena appearing in nonlinear systems. During the process, strong interactions among the system components lead to long-range ordering and the formation of spatial structures. This effect plays a crucial role in a broad

context, from biology [1–4], chemistry [5, 6] and hydrodynamics [7] to soft-matter physics [8–11].

In optics the spontaneous formation of regular intensity patterns has been observed almost 30 years ago [12], and since been explored in various settings [13, 14]. Common to all these experiments is the requirement of an appropriate feedback mechanism, provided e.g. by an optical cavity or a single mirror that retro-reflects traversing light back into the medium.

On the other hand, the formation of spatial structures solely due to the nonlinear propagation of light has attracted great interest over the past years [15–17]. Most prominently, optical solitons emerging from local Kerr-type nonlinearities of various kinds have been actively investigated [18–20] and play an important role for intense light propagation [21] and potential applications to fiber optics communication [22]. Nonlinearities can cause extended structures to emerge, e.g., from modulation instabilities (MI) that drive a growth of broad-band intensity or density modulations and ultimately lead to the formation of randomly arranged filaments [23–26].

In this work, we follow up on [17] and deepen the investigation of self-organization into spatially ordered patterns in the framework of the nonlinear Schrödinger equation with competing nonlocal nonlinearities. Competing nonlinearities occur whenever few different physical processes contribute to the nonlinear response. For example, light propagation in nematic liquid crystals that exhibits both thermal as well as reorientational nonlocal nonlinearities [27, 28] or, light propagation in thermal alkali metal vapor [17]. In the latter case, nonlocality arises from the diffusive atomic motion and, the simultaneous coupling of light to near-resonant transitions involving two incoherently coupled hyperfine levels can give rise to competing nonlinearities. Here, we will employ competing *Gaussian nonlocal* nonlinearities. While such model does not directly represent a real-world physical response, in the literature it is often used as a toy-model for nonlocality and is very well suited for illustrative purposes. The competition between the attractive and repulsive Gaussian responses may lead to a sign flip of the total response in Fourier

***Corresponding Author: F. Maucher:** Joint Quantum Centre (JQC) Durham-Newcastle, Department of Physics, Durham University, Durham DH1 3LE, United Kingdom; Department of Mathematical Sciences, Durham University, Durham DH1 3LE, United Kingdom, E-mail: fabian.maucher@durham.ac.uk

T. Pohl: Max Planck Institute for the Physics of Complex Systems, 01187 Dresden, Germany

W. Krolikowski: Laser Physics Centre, Research School of Physics and Engineering, Australian National University, Canberra, ACT 0200, Australia; Science Program, Texas A&M University at Qatar, Doha, Qatar

S. Skupin: Univ. Bordeaux - CNRS - CEA, Centre Lasers Intenses et Applications, UMR 5107, 33405 Talence, France; Univ Lyon, Université Claude Bernard Lyon 1, CNRS, Institut Lumière Matière, F-69622, VILLEURBANNE, France

space [29], which in the present case drives MI within a finite band [30] of momenta [see Fig. 1(b,c)].

Furthermore, we find a crucial dependence of the order of the phase-transition from unordered to ordered state on the transverse dimensionality of the system. This dependence is a generic property of amplitude equations, which has already been found in a range of other systems [31].

2 Model

We study the propagation of the wave function $\psi(\mathbf{r}, z)$, which represents, for example, the slowly varying envelope of the main component of a linearly polarized light beam. We assume that its dynamics can be described by the nonlinear Schrödinger equation with nonlocal nonlinearity characterized by the response function $R(r)$,

$$i\partial_z\psi(\mathbf{r}, z) = -\Delta_{\perp}^{(n)}\psi(\mathbf{r}, z) - \int R(|\mathbf{r} - \mathbf{r}'|)|\psi(\mathbf{r}', z)|^2 d^n r' \psi(\mathbf{r}, z). \quad (1)$$

Here, \mathbf{r} and z denote transverse and longitudinal (propagation) coordinates, respectively, $n = 1, 2$ the dimensionality of the transverse coordinates \mathbf{r} , and $\Delta_{\perp}^{(n)} = \partial_{xx} + \partial_{yy}$ for $n = 2$ or $\Delta_{\perp}^{(n)} = \partial_{xx}$ for $n = 1$, respectively. We consider a competing Gaussian response for the nonlocal cubic nonlinearity, i.e.

$$R(r) = \begin{cases} \alpha\sigma\sqrt{\pi}e^{-\frac{r^2}{\sigma^2}} - \sqrt{\pi}e^{-r^2}, & \text{for } n = 1 \\ \alpha e^{-\frac{r^2}{\sigma^2}} - e^{-r^2}, & \text{for } n = 2 \end{cases} \quad (2)$$

with $r^2 = x^2$ for $n = 1$, and $r^2 = x^2 + y^2$ for $n = 2$. The specific form of the response Eq. (2) with two degrees of freedom α, σ can be achieved by rescaling amplitude and length scales in Eq. (1) appropriately. The two parameters describe strength ($0 < \alpha < 1$) and extent ($0 < \sigma < 1$) of the focusing part of nonlinear response. The second term of the response Eq. (2) $\propto \exp(-r^2)$ is the defocusing part of the response and does not contain any free parameter. Given that $0 < \alpha, \sigma < 1$, the total response Eq. (2) is defocusing everywhere in position space, and the defocusing part of the response is broader than the focusing one.

The Fourier transform $\tilde{R}(k)$ of $R(r)$ for both transverse dimensionalities $n = 1, 2$ is given by

$$\tilde{R}(k) = \alpha\pi\sigma^2 e^{-\frac{\sigma^2 k^2}{4}} - \pi e^{-\frac{k^2}{4}}, \quad (3)$$

with $k^2 = k_x^2$ for $n = 1$, and $k^2 = k_x^2 + k_y^2$ for $n = 2$. Because of our particular choice of parameter ranges $0 < \alpha, \sigma < 1$,

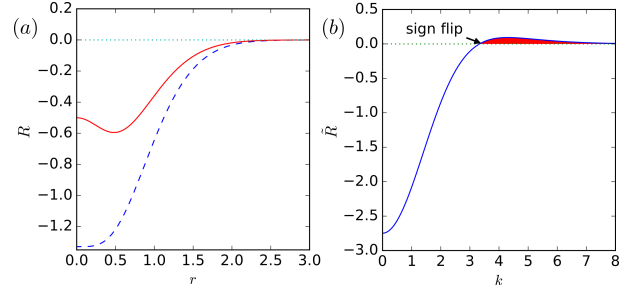


Figure 1: (colour online) (a) Drawing of the response Eq. (2) for $n = 1$ (blue dashed line) and $n = 2$ (red solid line) and (b) its Fourier transform Eq. (3) for $\alpha = 1/2, \sigma = 1/2$. Whereas the response in position space is negative everywhere, the competition between the two Gaussian responses leads to a node in Fourier domain.

$\tilde{R}(k)$ takes a negative value at $k = 0$. Moreover,

$$\partial_k^2 \tilde{R}(k)|_{k=0} = \frac{\pi}{2} (1 - \alpha\sigma^4) > 0 \quad (4)$$

implies that this negative value at origin is a minimum of $\tilde{R}(k)$. On the other hand, it is easy to verify that the function $\tilde{R}(k)$ has a real-valued node $\tilde{R}(k_0) = 0$ at

$$k_0 = 2\sqrt{\frac{\ln(\alpha\sigma^2)}{\sigma^2 - 1}}, \quad (5)$$

and takes only positive values for $k > k_0$. This property turns out to be crucial for the MI properties as explained in the next section. The typical shape of the response is shown in Fig. 1 for $\alpha = 1/2, \sigma = 1/2$.

3 Modulational Instability

Modulational instability (MI) refers to the propagation dynamics of small periodic amplitude modulations $a(\mathbf{r}, z) = a_1 \exp(i\mathbf{k}\mathbf{r} + \lambda z) + a_2^* \exp(-i\mathbf{k}\mathbf{r} + \lambda^* z)$ of an otherwise constant plane wave background $\psi_{\text{pw}} = \sqrt{\mathcal{J}} \exp(i\mu z)$ with $\mu = \mathcal{J} \int R(\mathbf{r}) d^2 r$. Then, MI means that this perturbation grows exponentially upon propagation, $a(\mathbf{r}, z) \propto \exp(\lambda z)$. The associated growth rate λ , for both of the cases $n = 1, 2$ can be found by linearisation of Eq. (1) with respect to the small amplitudes $a_{1,2}$, and is given by

$$\lambda^2 = -k^2 \mathcal{J} \left(\frac{k^2}{\mathcal{J}} - 2\tilde{R}(k) \right). \quad (6)$$

This formula implies that whenever $\lambda^2 > 0$ and thus $\left(\frac{k^2}{\mathcal{J}} - 2\tilde{R}(k) \right) < 0$ we find exponentially growing solutions and thus MI. Hence, whenever there is an interval, for which we have $\tilde{R}(k) > 0$ [see Fig. 1(b)], it is clear that by choosing \mathcal{J} sufficiently large and thus making the parabola k^2/\mathcal{J} shallower, we can expect MI in a certain k -range. The

critical background intensity \mathcal{J}_{MI} above which MI occurs depends on the parameters α, σ . At intensities above \mathcal{J}_{MI} , MI is restricted to an interval around a certain wavenumber k_{MI} . The situation is sketched in Fig. 2 for fixed values $\alpha = 1/2$ and $\sigma = 1/2$, for which one finds $\mathcal{J}_{\text{MI}} \approx 92.0$ and $k_{\text{MI}} \approx 4.00$. If the response R is defocusing and sign-definite in Fourier space, it is clear that there is no solution to $\lambda^2 > 0$ at all. On the other hand, if the response R were focusing [$\tilde{R}(0) > 0$], we would find modulational instability near $k = 0$ for arbitrarily small intensities. Then, so-called long-wave modulational instability would give rise to filamentation at random positions and formation of bright solitons or collapse [32, 33]. However, given that we already excluded the focusing case by choosing $0 < \alpha, \sigma < 1$, we will not discuss it any further in the following. For our purposes, it is crucial that MI occurs around a finite wavenumber $k_{\text{MI}} > k_0 > 0$, so that there is only a finite band of wavelengths for which we find MI. Thus, only perturbations in this k -range are allowed to grow and an additional length scale is imposed on the system. It is important to note that this MI scenario does not depend on the dimensionality, since Eq. (6) and \tilde{R} do not depend on n .

The typical shape of $-\lambda^2(k)$ is a (local) maximum followed by a (local) minimum [see Fig. 2(a)]. This so-called maxon-roton structure is well-known for the excitation spectrum of superfluid Helium [34, 35], and studied for Bose-Einstein condensates with finite-range interactions [36–38]. The roton minimum and the associated instability in quantum fluids may appear as a precursor to a solid phase [39, 40], but can also usher in a transition to a modulated fluid described by a single-particle amplitude ψ [37, 41]. The so-called roton gap can be defined as the value of $-\lambda^2(k)$ at the previously mentioned minimum $\min_k(-\lambda^2)$, which is positive in the case of $\mathcal{J} < \mathcal{J}_{\text{MI}}$ [see Fig. 2(a)].

4 Ground states and phase-transition

Let us define the ground state of our system as the minimizer of the energy functional/Hamiltonian \mathcal{E} :

$$\begin{aligned} \mathcal{E} = & \frac{1}{V} \int_V |\nabla \psi(\mathbf{r})|^2 d^n r \\ & - \frac{1}{2V} \iint_V R(\mathbf{r} - \mathbf{r}') |\psi(\mathbf{r})|^2 |\psi(\mathbf{r}')|^2 d^n r' d^n r \end{aligned} \quad (7)$$

Here, V stands for the volume of the integration area, that has the dimensionality of the transverse coordinates, and

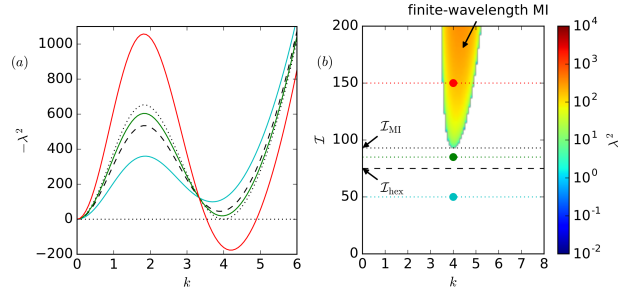


Figure 2: (colour online) Figure (a) shows $-\lambda^2$ as function of k for different values of intensity $\mathcal{J} = 50, 85, 150$ and $\alpha = 1/2, \sigma = 1/2$. The solid coloured curves correspond the intensities $\mathcal{J} = 50, 85, 150$. The dotted black line that just touches the zero corresponds to the critical intensity \mathcal{J}_{MI} , above which one finds MI. The other black dashed line is discussed in section 4. It shows, that the phase transition in two transverse dimensions occurs at finite roton gap. The colour plot (b) depicts the (\mathcal{J}, k) -region, where $\lambda^2 > 0$. Intensities from (a) are indicated as lines in the same color coding.

we are interested in the limit $V \rightarrow \infty$. For practical purposes, V represents the size of the (sufficiently large) transverse numerical box, i.e. $V = l_x$ in case of $n = 1$ and $V = l_x l_y$ in case of $n = 2$. The energy \mathcal{E} is conserved upon propagation, i.e., $\partial_z \mathcal{E} = 0$. Furthermore, let us introduce the chemical potential/propagation constant μ by

$$\begin{aligned} \mu = & -\frac{1}{\int_V |\psi|^2 d^n r} \int_V |\nabla \psi(\mathbf{r})|^2 d^n r \\ & + \frac{1}{\int_V |\psi|^2 d^n r} \iint_V R(\mathbf{r} - \mathbf{r}') |\psi(\mathbf{r})|^2 |\psi(\mathbf{r}')|^2 d^n r' d^n r \end{aligned} \quad (8)$$

In case of a defocusing nonlocal nonlinearity, for sufficiently small background intensity the ground state is a plane wave that is stable [see Eq. (6)]. On the other hand, when increasing the background intensity, there is a critical value \mathcal{J}_{cr} above which the plane wave solution is no longer the ground state of the system. That can be anticipated from the fact, that a plane wave is linearly unstable above \mathcal{J}_{MI} . Thus, when sweeping through \mathcal{J} we should find a point at which the system undergoes a phase-transition from plane wave to some other (spatially modulated) ground state.

It is tempting to assume that this critical intensity \mathcal{J}_{cr} coincides with the threshold intensity \mathcal{J}_{MI} above which we find MI, and that therefore this critical intensity \mathcal{J}_{cr} does not depend on the dimensionality of the system. However, both of these assertions are wrong in general. Since MI relies on linearisation, it is a sufficient, but not necessary criterion for finding a modulated ground state. To find the spatially modulated ground state, one has to solve a full nonlinear problem, i.e. minimize the energy functional Eq. (7). Thus, it can be anticipated that the actual

critical intensity \mathcal{J}_{cr} , at which the phase-transition occurs, can be lower than the critical intensity for MI, $\mathcal{J}_{\text{cr}} < \mathcal{J}_{\text{MI}}$. In other words, the phase-transition may happen at finite roton gap [see Fig. 2(a)].

We will show in the following two subsections, that the conditions for the existence of a spatially structured ground state depend crucially on the transverse dimensionality n of the system. In case of one transverse dimension, we find indeed that $\mathcal{J}_{\text{cr}} = \mathcal{J}_{\text{MI}}$, and the phase transition is of second order (and at vanishing roton gap), whereas in case of two transverse dimensions, $\mathcal{J}_{\text{cr}} < \mathcal{J}_{\text{MI}}$, and the phase transition is of first order (and at finite roton gap).

4.1 Ground states and phase-transition with one transverse dimension ($n = 1$)

To determine the ground state ψ_{gs} we solve Eq. (1) for an imaginary propagation coordinate ($z \rightarrow -iz$) with periodic boundary condition, starting from a plane wave perturbed by small amplitude white noise $\varepsilon(\mathbf{r})$, $\psi(\mathbf{r}, 0) = \mathcal{J}^{1/2} + \varepsilon(\mathbf{r})$. Fig. 3(a-c) show numerically exact ground states for different intensities and $\alpha = \sigma = 1/2$. In Fig. 3(d) the dependence of the energy difference $\mathcal{E}_{\text{gs}} - \mathcal{E}_{\text{pw}}$ as function of the intensity are illustrated. Clearly, the intensity \mathcal{J}_{mod} at which the phase transition from plane wave to modulated ground state occurs, is exactly the same as \mathcal{J}_{MI} . Hence, the phase transition happens at a vanishing roton gap ($\min_{\mathbf{k}}(-\lambda^2) = 0$). Furthermore, given that μ is continuous at the point of phase transition, it is clear that this constitutes a second order phase transition.

4.2 Ground states and phase-transition with two transverse dimensions ($n = 2$)

In Fig. 4(a-c) we show numerically exact ground states for different background intensities, $\alpha = \sigma = 1/2$, and $n = 2$. Unlike the one-dimensional case discussed in preceding section, in this case we see that the intensity \mathcal{J}_{hex} at which the phase transition to the modulated state happens is smaller than the critical intensity for modulational instability, $\mathcal{J}_{\text{hex}} < \mathcal{J}_{\text{MI}}$. Thus, the phase transition occurs at a finite roton gap [compare to the dashed line in Fig. 2(a)]. Furthermore, intensity modulations in ψ_{gs} set in abruptly upon crossing \mathcal{J}_{hex} rather than growing continuously. This behaviour is consistent with a first order phase transition as expected for two-dimensional systems [38, 42]. The label \mathcal{J}_{hex} was used, since in the two dimensional case the pattern corresponds to a hexagonal structure. The fact that

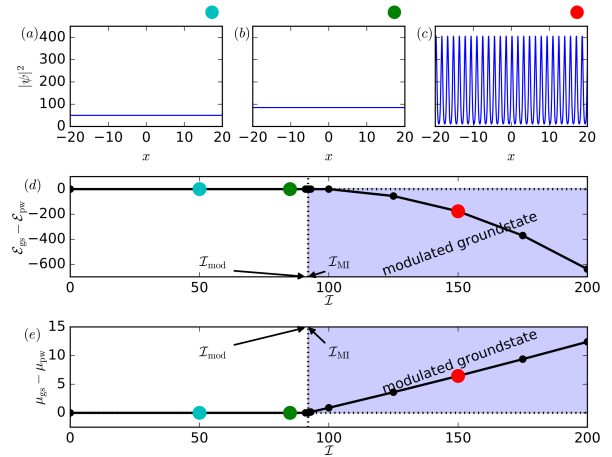


Figure 3: (colour online) (a-c) show ground states for different intensities $\mathcal{J} = 50, 85, 150$ and $\alpha = 1/2, \sigma = 1/2$ (compare to Fig. 2). Figure (d) shows the difference of the energy between the numerically exact ground state and the plane wave as function of the intensity. Thus, the intensity \mathcal{J}_{mod} at which the line $\mathcal{E}_{\text{gs}}(\mathcal{J}) - \mathcal{E}_{\text{pw}}(\mathcal{J})$ starts to deviate from zero marks the point at which the phase transition from plane wave to modulated ground states occurs. Clearly, $\mathcal{J}_{\text{mod}} = \mathcal{J}_{\text{MI}}$, and thus the phase transition occurs at vanishing roton gap (see Fig. 2). Figure (e) shows, that the chemical potential μ does not jump at the point of the phase transition, thus the phase transition is of second order.

the phase transition is now of first order is also visible by the sharp jump in the chemical potential μ . Hence, there is a clear dependence of the phase-transition on the transverse dimensionality of the system, which cannot be anticipated from the behaviour of the growth rate Eq. (6) alone. We attribute this feature to the hexagonal symmetry of the two-dimensional ground state, which is dependent the direction of the wave vector \mathbf{k} , whereas Eq. (6) is isotropic, i.e., independent of the direction of the wave vector \mathbf{k} .

5 Accessing ordered states by unidirectional propagation

From a broader perspective, it is of crucial importance to know whether such spatially modulated states could be dynamically accessed by mere unidirectional propagation of an initial plane wave, and whether these states will actually approach a state that resembles the ground state. For that matter, we added small amplitude modulations at $z = 0$. Considering both transverse and propagational random perturbations would lead to random walk [43] and radiative losses [44], that for sufficiently small perturbation amplitude should not change the results qualitatively

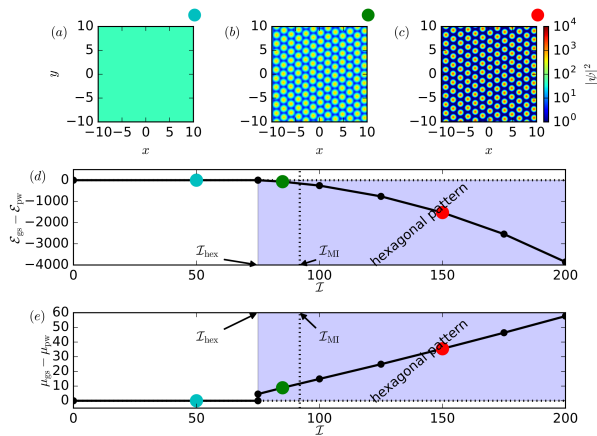


Figure 4: (colour online) (a-c) show ground states for different background intensities J and $\alpha = 1/2$, $\sigma = 1/2$. Graph (d) shows the energy difference between the exact plane wave state and the numerically found hexagonal pattern, as function of the intensity. Clearly, the phase transition occurs for smaller intensity than the threshold intensity for MI [compare to the dashed line in Fig. 2(a)]. Graph (e) shows that the chemical potential μ is discontinuous at the point of the phase transition, thus the latter is of first order.

due to the smoothing effect of the nonlocal nonlinearity, yet is beyond the scope of this paper. In case of one transverse dimension, the situation is illustrated in Fig. 5. In case of sufficiently large background intensity Fig. 5(c-d), the propagated amplitude clearly transforms into spatially periodic pattern, which appears to approach the numerically exact ground state. That dynamics, however, seems to be precluded by the fact, that we are considering an energy-conserving system $\partial_z \mathcal{E} = 0$, and thus the energy difference between the initial state (i.e. the plane wave) and the final state (i.e. modulated state) has to be zero. The way, how the system “dissipates” the surplus energy compared to the modulated ground state, $\delta \mathcal{E} = \mathcal{E}(\psi_{\text{initial}}) - \mathcal{E}(\psi_{\text{gs}})$, is by depositing energy in phase fluctuations of the wavefunction and thus increasing the kinetic energy. These phase fluctuations allow the amplitude profile to approach the amplitude profile of the numerically exact ground state.

In case of two transverse dimensions Fig. 6, we find a similar behaviour. As the beam propagates, it experiences a dynamic transformation leading to the formation of the hexagonal intensity pattern. Again, the way how the system “dissipates” the surplus energy $\delta \mathcal{E}$ is by depositing a large fraction of the surplus energy of the initial wavefunction to kinetic energy, clearly visible in the phase pattern in the right column in Fig. 6, where in this case vortices are formed upon propagation.

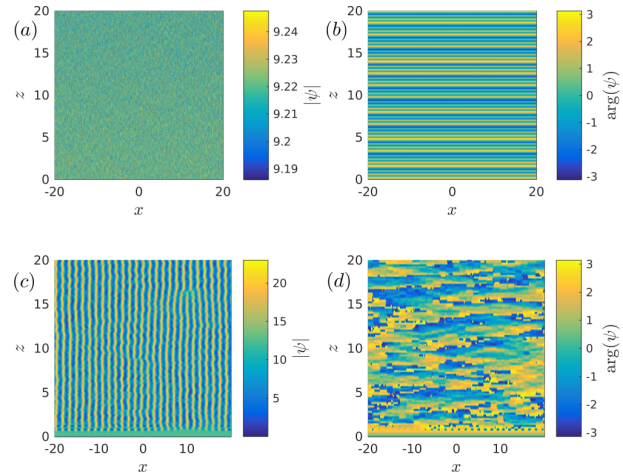


Figure 5: (colour online) Propagation dynamics for $J = 85$ (upper panel) and $J = 150$ (lower panel). If the intensity is below the threshold for MI, phase coherence in the transverse plane is maintained upon propagation (b), and no modulations build up in the intensity (a). On the other hand, if the intensity is larger than the threshold for MI, filaments form. After short distance (c), phase coherence between the formed filaments is destroyed upon propagation (d). The additional phase fluctuations allow to “dissipate” the surplus energy of the initial state, so that the amplitude profile of the propagating beam can approach the amplitude profile of the numerically exact ground state that has a flat phase.

6 Conclusions

We used a competing Gaussian nonlocal nonlinear response as a simple toy model to illustrate the ability of the nonlinear Schrödinger equation to support spatially modulated ground states. Our results confirm that the formation of such regular intensity patterns is a generic property of media with competing nonlocal nonlinearities, and does not critically depend on detailed form of the nonlocal response, as long as the Fourier transform of the response has a node at some positive k and a negative value at $k = 0$ to avoid soliton formation or even collapse. Furthermore, we illustrated how the order of the phase transition crucially depends on the transverse dimensionality of the system. Finally, we investigated how hexagonal lattices of filaments can be accessed dynamically by mere unidirectional propagation, despite of the fact that we are considering an energy conserving system. We discussed that a crucial feature of the dynamics is the “dissipation” of energy into kinetic energy by formation of phase fluctuations or vortices (depending on the transverse dimensionality), so that the amplitude profile of the propagating beam can approach the numerically exact ground state.

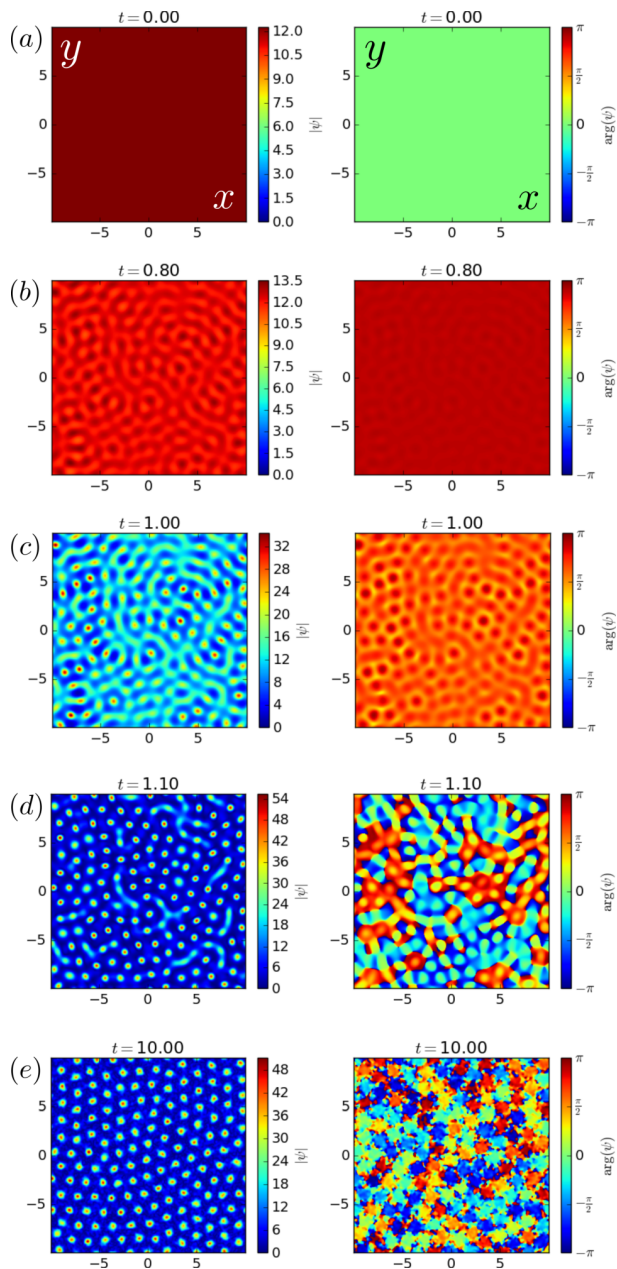


Figure 6: (colour online) Accessing patterns composed of hexagonal lattice of filaments by free unidirectional propagation ($\alpha = 1/2$, $\sigma = 1/2$). First, the initial plane wave (a) undergoes modulational instability which leads to small amplitude modulations upon propagation (b). These amplitude modulations grow further and start creating strongly interacting filaments (c-d). Finally, these strongly interacting filaments self-arrange into a hexagonal lattice and approach the amplitude profile of the exact groundstate. The phase of the propagated wavefunction contains vortices and accounts for the energy difference between the initial flat state and the hexagonal pattern (with flat phase). See also the supplementary movie `gauss_pattern.mp4`.

Acknowledgement: Numerical simulations were performed using computing resources at Mésocentre de Calcul Intensif Aquitain (MCIA) and Grand Equipement National pour le Calcul Intensif (GENCI, Grant No. 2016-056129 and 2016-057594). This work was partially supported by the EU through FET-grants HAIRS 612862 and QuILMI 295293 and by the Qatar National Research Fund through the National Priorities Research Program (Grant No. NPRP 8-246-1-060). F. M. acknowledges funding by the Leverhulme Trust Research Programme Grant RP2013-K-009.

References

- [1] J. D. Murray, *Mathematical Biology II: Spatial Models and Biomedical Applications* (Springer-Verlag Berlin Heidelberg, 1993).
- [2] S. Camazine, J.-L. Deneubourg, R. F. Nigél, J. Sneyd, G. Theraulaz, and E. Bonabeau, *Self-organization in biological systems* (Princeton University Press, 2001).
- [3] M. Rietkerk, S. C. Dekker, P. C. de Ruiter, and J. van de Koppel, *Science* **305**, 1926 (2004).
- [4] D. Escaff, C. Fernandez-Oto, M. G. Clerc, and M. Tlidi, *Phys. Rev. E* **91**, 022924 (2015).
- [5] E. Meron, *Phys. Rep.* **218**, 1 (1992).
- [6] V. Petrov, Q. Ouyang, and H. Swinney, *Nature* **388**, 655 (1997).
- [7] A. C. Newell, T. Passot, and J. Lega, *Annu. Rev. Fluid Mech.* **25**, 399 (1993).
- [8] C. Likos, *Phys. Rep.* **348**, 267 (2001).
- [9] M. Leunissen, C. Christova, A. Hynninen, C. Royall, A. Campbell, A. Dijkstra, R. van Roij, and A. van Blaaderen, *Nature* **437**, 7056 (2005).
- [10] Y. H. Liu, L. Y. Chew, and M. Y. Yu, *Phys. Rev. E* **78**, 066405 (2008).
- [11] F. Maucher and P. Sutcliffe, *Phys. Rev. Lett.* **116**, 178101 (2016).
- [12] G. Grynberg, E. Le Bihan, P. Verkerk, P. Simoneau, J. Leite, D. Bloch, S. LeBoiteux, and M. Ducloy, *Opt. Commun.* **67**, 363 (1988).
- [13] F. T. Arecchi, S. Boccaletti, and P. Ramazza, *Phys. Reports* **318**, 83 (1999).
- [14] A. Camara, R. Kaiser, G. Labeyrie, W. J. Firth, G. L. Oppo, G. R. M. Robb, A. S. Arnold, and T. Ackemann, *Phys. Rev. A*, 013820 (2015).
- [15] S. Trillo and W. Torruellas, eds., *Spatial Solitons* (Springer, Berlin, 2001).
- [16] Y. Kivshar and G. Agrawal, *Optical Solitons: From Fibers to Photonic Crystals* (Academic Press, 2003).
- [17] F. Maucher, T. Pohl, S. Skupin, and W. Krolikowski, *Phys. Rev. Lett.* **116**, 163902 (2016).
- [18] M. Quiroga-Teixeiro and H. Michinel, *J. Opt. Soc. Am. B* **14**, 2004 (1997).
- [19] B. A. Malomed, L.-C. Crasovan, and D. Mihalache, *Physica D* **161**, 187 (2002).
- [20] J. Corney and O. Bang, *Phys. Rev. E* **64**, 047601 (2001).
- [21] A. Couairon and A. Mysyrowicz, *Phys. Rep.* **441**, 47 (2007).

- [22] G. P. Agrawal, *Nonlinear Fiber Optics*, 3rd ed. (Academic Press, San Diego, 2001).
- [23] A. V. Mamaev, M. Saffman, D. Z. Anderson, and A. A. Zozulya, *Phys. Rev. A* **54**, 870 (1996).
- [24] M. Saffman, G. McCarthy, and W. Krolikowski, *J. Opt. B* **6**, S397 (2004).
- [25] J. Meier, G. I. Stegeman, D. N. Christodoulides, Y. Silberberg, R. Morandotti, H. Yang, G. Salamo, M. Sorel, and J. S. Aitchison, *Phys. Rev. Lett.* **92**, 163902 (2004).
- [26] S. Henin, Y. Petit, J. Kasparian, J.-P. Wolf, A. Jochmann, S. Kraft, S. Bock, U. Schramm, R. Sauerbrey, W. Nakaema, K. Stelmaszczyk, P. Rohwetter, L. Wöste, C.-L. Soulez, S. Mauger, L. Bergé, and S. Skupin, *App. Phys. B* **100**, 77 (2010).
- [27] J. F. Warengem, M. Blach and J. F. Henninot, *Mol. Cryst. Liq. Cryst.* **454**, 297 (2006).
- [28] M. Warengem, J. F. Blach, and J. F. Henninot, *J. Opt. Soc. Am. B* **25**, 1882 (2008).
- [29] C. N. Likos, B. M. Mladek, D. Gottwald, and G. Kahl, *J. Chem. Phys.* **126**, 224502 (2007).
- [30] B. K. Esbensen, A. Wlotzka, M. Bache, O. Bang, and W. Krolikowski, *Phys. Rev. A* **84**, 053854 (2011).
- [31] M. C. Cross and P. C. Hohenberg, *Rev. Mod. Phys.* **65**, 851 (1993).
- [32] V. I. Bespalov and V. I. Talanov, *JETP Lett.* **3**, 471 (1966).
- [33] L. Bergé, *Phys. Rep.* **303**, 259 (1998).
- [34] L. Landau, *Phys. Rev.* **60**, 356 (1941).
- [35] R. P. Feynman and M. Cohen, *Phys. Rev.* **102**, 1189 (1956).
- [36] L. Santos, G. V. Shlyapnikov, and M. Lewenstein, *Phys. Rev. Lett.* **90**, 250403 (2003).
- [37] N. Henkel, R. Nath, and T. Pohl, *Phys. Rev. Lett.* **104** (2010).
- [38] T. Macri, F. Maucher, F. Cinti, and T. Pohl, *Phys. Rev. A* **87**, 061602 (2013).
- [39] T. Schneider and C. P. Enz, *Phys. Rev. Lett.* **27**, 1186 (1971).
- [40] G. E. Astrakharchik, J. Boronat, I. L. Kurbakov, and Y. E. Lozovik, *Phys. Rev. Lett.* **98**, 060405 (2007).
- [41] F. Cinti, T. Macri, W. Lechner, G. Pupillo, and T. Pohl, *Nature Comm.* **5**, 3235 (2014).
- [42] F. Cinti, M. Boninsegni, and T. Pohl, *New. J. Phys.* **16**, 033038 (2014).
- [43] V. Folli and C. Conti, *Phys. Rev. Lett.* **104**, 193901 (2010).
- [44] F. Maucher, W. Krolikowski, and S. Skupin, *Phys. Rev. A* **85**, 063803 (2012).